Electronic Supplementary Materials

“Setaria viridis”–like cobalt complexes derived Co/N-doped carbon nanotubes as efficient ORR/OER electrocatalyst for long-life rechargeable Zn-air batteries

Shicheng Yi,[#] Rong Xin,[#] Xuxin Li, Yuying Sun, Mei Yang, Bei Liu, Hongbiao Chen, Huaming Li, Yijiang Liu*

College of Chemistry and Key Laboratory of Environmentally Friendly Chemistry and Application of Ministry of Education, Xiangtan University, Xiangtan 411105, Hunan Province, China

Corresponding author: liuyijiang84@xtu.edu.cn

[#] Shicheng Yi and Rong Xin contributed equally to this work.

1. Experimental section

1.1 Materials

Multi wall carbon nanotubes (MWCNT) and $Co(NO_3)_2$ $6H_2O$ were purchased from the Aladdin Biochemical Technology Co., Ltd. Melamine (Mel) was purchased from the Sinopharm Chemical Reagent Co., Ltd. All the chemical regents were used as received without any further purification.

1.2 Synthesis of Co-CNT and N-CNT

The reference Co-CNT was prepared with the similar method as Co/N-CNT. Briefly, 0.06 g of HMWCNT was thoroughly dispersed in 30 mL of methanol to form solution A under continuous ultrasonic. Meanwhile, 0.225 g of $Co(NO_3)_2$•$6H_2O$ was dissolved in 10 mL of methanol to get solution B. Subsequently, solution B was poured into solution A under stirring at 25 °C for 24 h to form the Co-HMWCNT composites, which was subsequentially calcinated at 800 °C for 2 h at a ramping rate of 3 °C/min under N_2 atmosphere. The final product was denoted as Co-CNT.

For the preparation of N-CNT, 0.50 g of melamine was dissolved in 30 mL of methanol to form solution B. The HMWCNT and melamine solution were then mixed, and stirred at 25 °C for 24 h to form the Mel-HMWCNT mixture. Afterward, N-CNT was obtained via an identical pyrolysis as Co-CNT.

1.3 *Characterization*

Scanning electron microscopy (SEM) was conducted on JSM-6610LV; Transmission electron microscopy (TEM) was performed on JEOL JEM-1101; X-ray diffraction analysis (XRD) was detected on U1tima IV using a Cu Kα (λ = 0.154 nm) radiation source; Raman spectrum was obtained on Via Raman microscope using a 633 nm laser source; N_2 adsorption-desorption isotherms were obtained on TriStar II 3020 and the specific surface area was calculated based on Barrette-Emmette-Teller (BET) theory; and X-ray photoelectron spectroscopy (XPS) was characterized on K-Alpha 1063.

1.4 Electrochemical measurements

In this experiment, the electrochemical measurements were conducted by an electrochemical workstation (CHI760D) with a typical three-electrode system. Ag/AgCl was selected as the reference electrode, graphite rod was used as the counter electrode, and rotating disk electrode (RDE) coated with the catalyst was treated as the working electrode. To prepare the catalyst inks, 4.0 mg catalyst samples were dispersed in a mixture solution of 750 μL ethanol solution, 200 μL deionized water and 50 μL 5 wt.% Nafion solution by sonication for 1 h. The ORR and OER performances were carried out with a rotation speed of 1,600 rpm in an O_2-saturated 0.1 M KOH. The air electrode was made of a carbon paper with 1.5 mg of Co/N-CNT catalyst. A polished Zn-foil was used as the anode; 6 M KOH solution dissolved with 0.2 M $Zn(Ac)_2$ was used as the electrolyte in the measurement. The solid state flexible air electrode was made of carbon cloth with 1.5 mg Co/N-CNT catalyst, sodium polyacrylate (PANa) alkaline hydrogel was used as the solid electrolyte.

The RRDE measurements were also conducted to determine the formed peroxide species and n. The ring-disk electrode was scanned at a rate of 10 mV s^{-1}. The yield of peroxide species (%HO_2^- in alkaline media) was calculated using the following equation:

$$\%\mathrm{HO_2^-} = 200 \times \frac{i_r / N}{i_r / N + i_d}$$

$$n = 4 \times \frac{i_d}{i_r / N + i_d}$$

where i_d and i_r are the disk and ring currents, respectively. N is the current collection efficiency of Pt ring, which was determined to be 0.37.

2. Figures

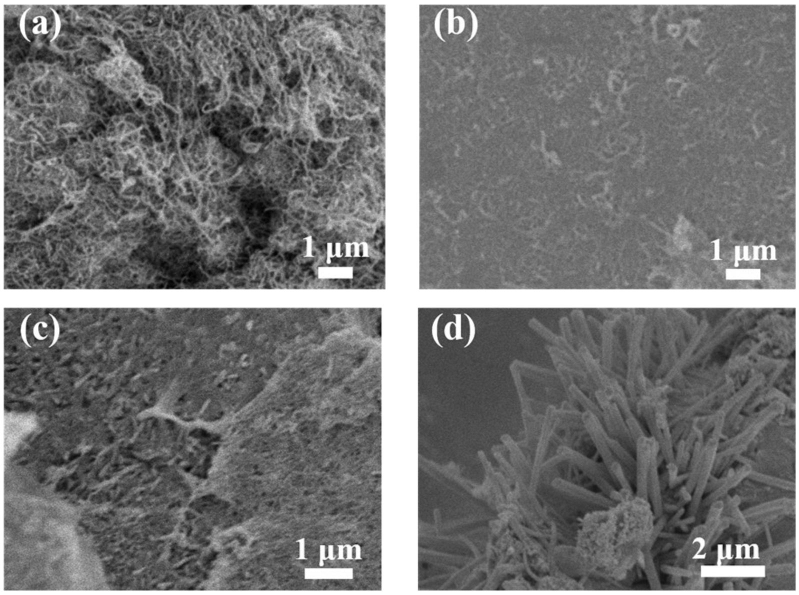

Fig. S1 SEM images of (a) MWCNT, (b) HMWCNT, (c) $Co_{0.67}$-Mel-HMWCNT and (d) $Co_{1.33}$-Mel-HMWCNT.

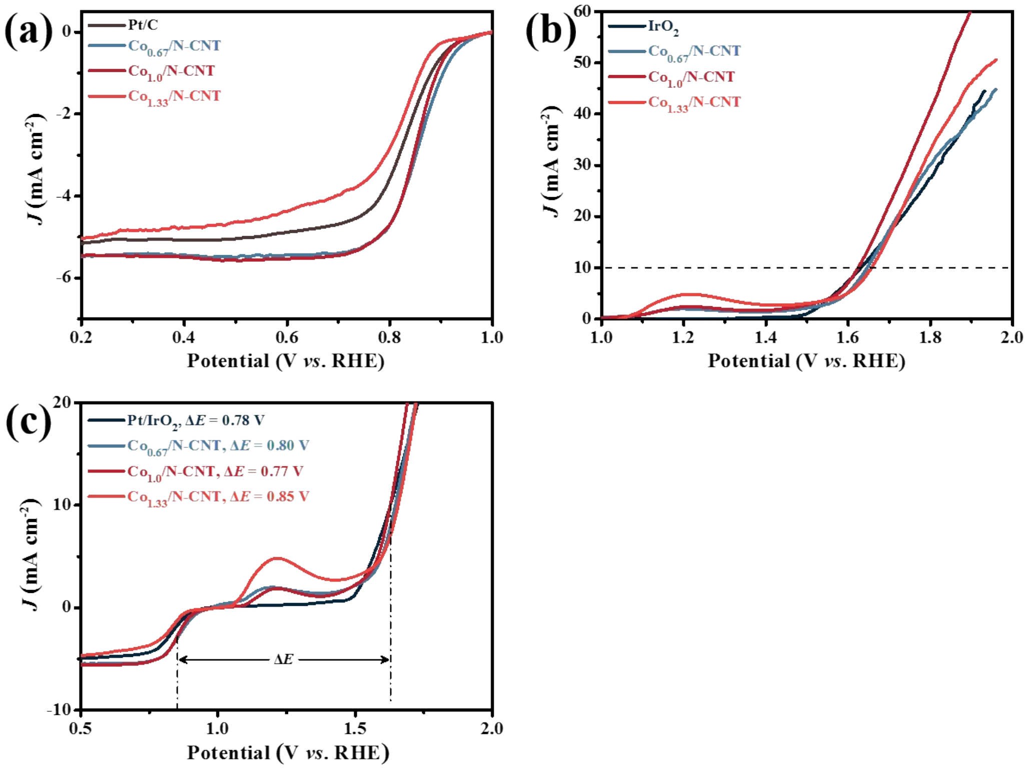

Fig. S2 LSV curves of 20% Pt/C, $Co_{0.67}$/N-CNT, $Co_{1.0}$/N-CNT, and $Co_{1.33}$/N-CNT electrocatalysts during ORR (a) and (b) OER; (c) The ORR/OER bifunctional LSV curves.

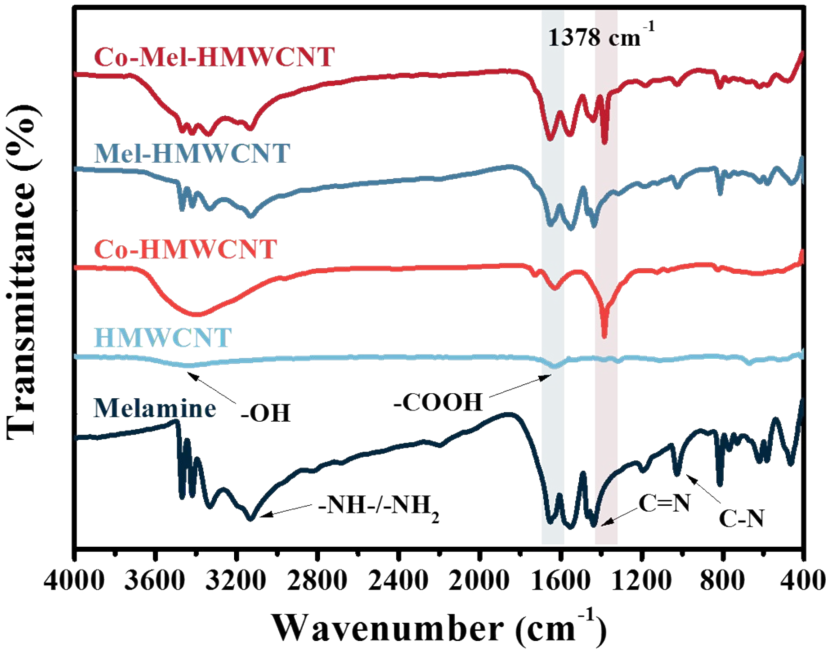

Fig. S3 FTIR spectra of the as-synthesized samples.

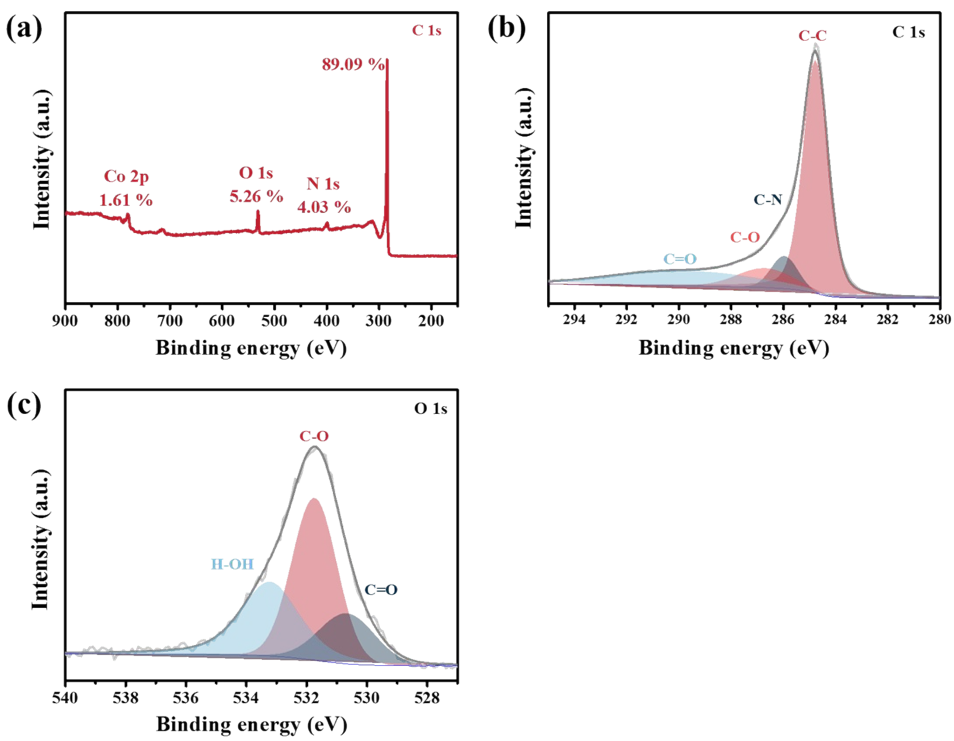

Fig. S4 (a) Full survey XPS spectrum and high-resolution XPS spectra of (b) C 1s and (c) O 1s of the Co/N-CNT.

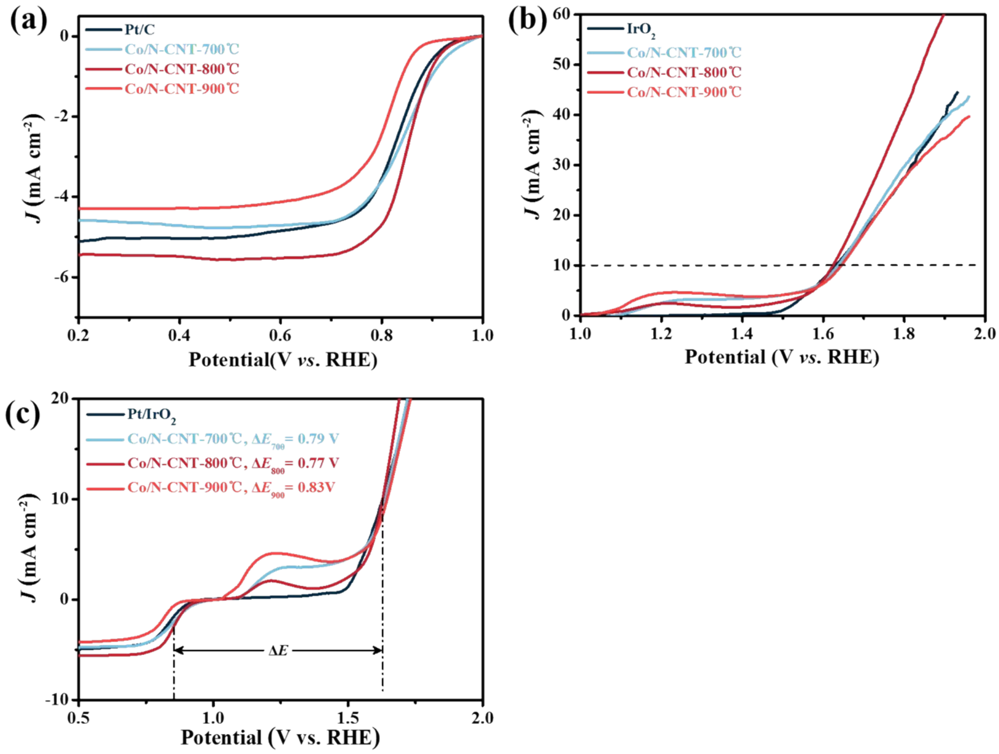

Fig. S5 LSV curves of 20% Pt/C, Co/N-CNT-700 °C, Co/N-CNT-800 °C, and Co/N-CNT-900 °C during (a) ORR and (b) OER; (c) The ORR/OER bifunctional LSV curves.

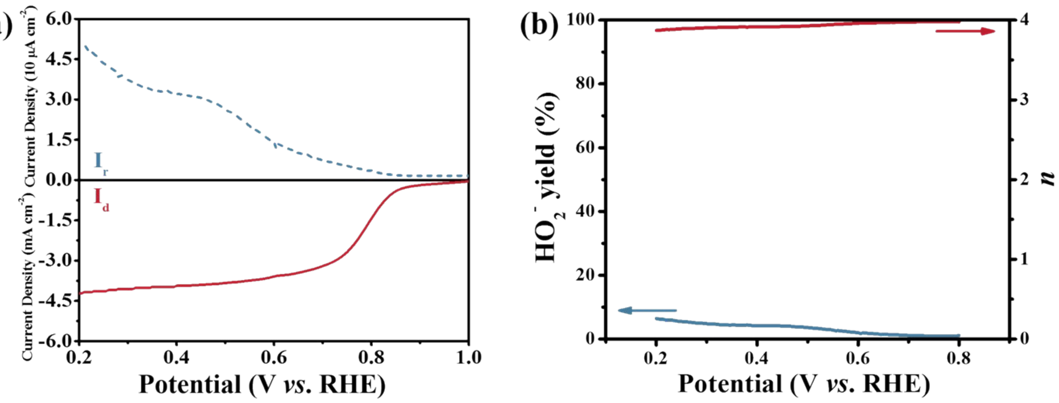

Fig. S6 (a) RRDE voltammograms of Co/N-CNT at 1600 rpm in 0.1 M KOH. (b) HO_2^- yield (%) and electron transfer number (n) according to the RRDE measurements in 0.1 M KOH.

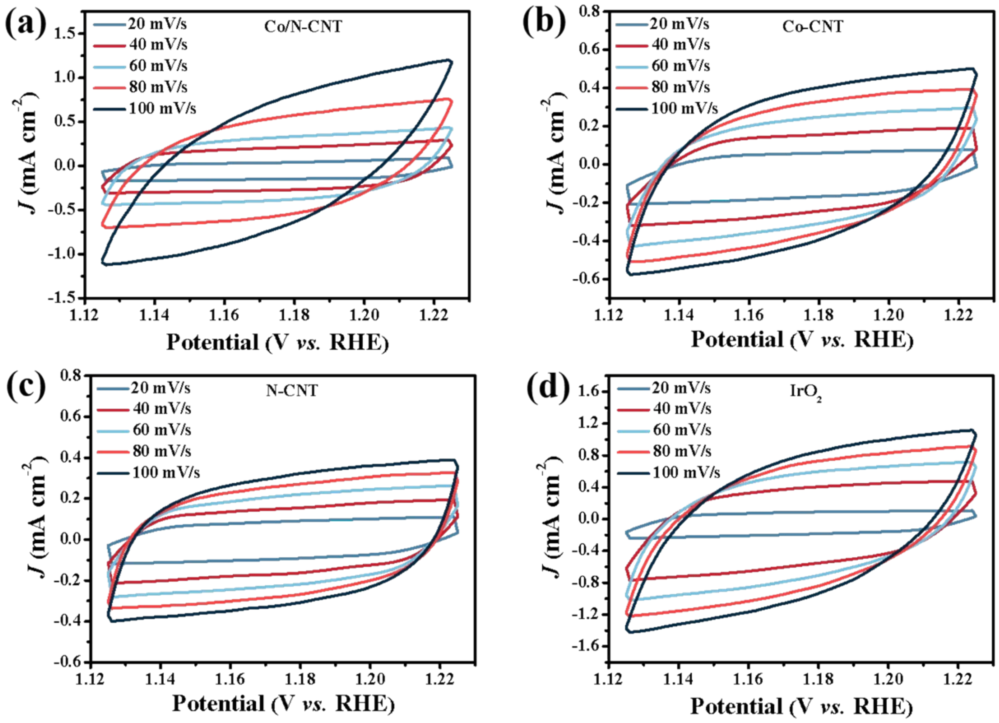

Fig. S7 Cyclic voltammetry (CV) curves of (a) Co/N-CNT, (b) Co-CNT, (c) N-CNT, and (d) IrO_2 in O_2-saturated 1.0 M KOH solution at different scan rates.

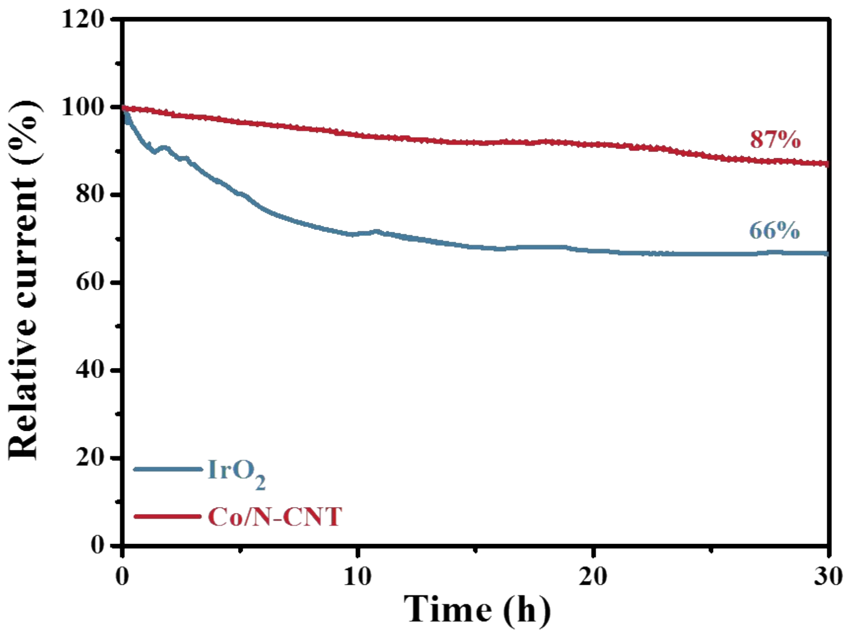

Fig. S8 Chronoamperometry curves of Co/N-CNT and IrO_2 electrocatalysts in O_2-saturated 0.1 M KOH electrolyte.

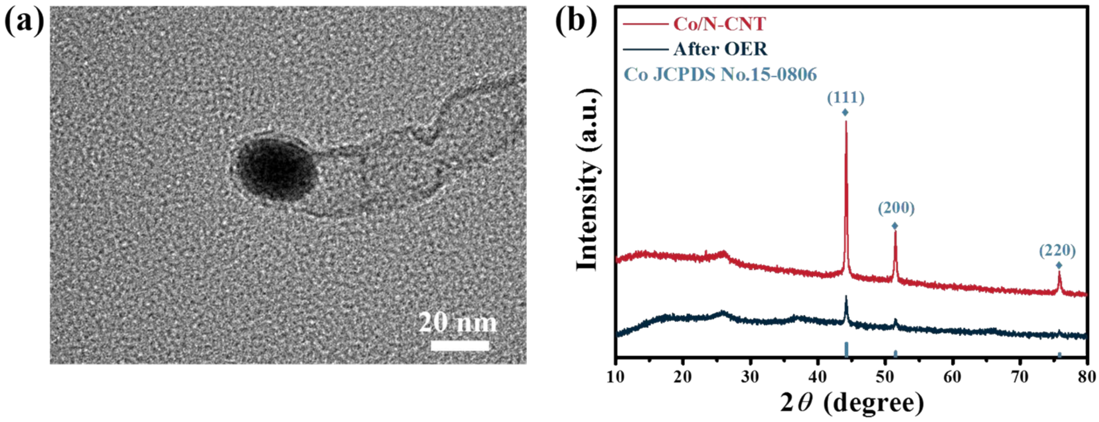

Fig. S9 (a) TEM images of Co/N-CNT after OER stability tests, (b) XRD patterns of Co/N-CNT before and after OER stability testing.

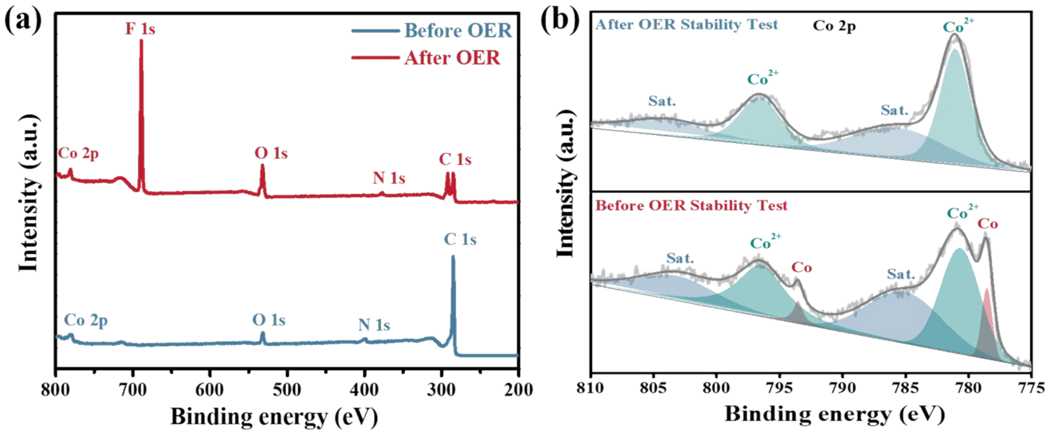

Fig. S10 (a) Full survey XPS spectrum and (b) high-resolution XPS spectra of Co 2p, of Co/N-CNT before and after OER stability test.

3. Tables

Table S1 ORR and OER performances of the as-synthesized electrocatalysts.

Catalysts	**ORR**			**OER**	**Δ*E***
	$J_{@0.4}$ **(mA cm^{-2})**	E_o **(V *vs*. RHE)**	$E_{1/2}$ **(V *vs*. RHE)**	$E_{j=10}$ **(V *vs*. RHE)**	
Co-CNT	3.56	0.88	0.79	1.65	0.86
N-CNT	4.68	0.94	0.84	1.74	0.90
Co/N-CNT	**5.47**	**0.97**	**0.85**	**1.62**	**0.77**
Pt/C	5.16	0.96	0.84	N/A	0.78
IrO_2	N/A	N/A	N/A	1.62	

Table S2 Comparison of the performances of Co/N-CNT electrocatalysts for ORR, OER and rechargeable aqueous ZAB with previously reported bifunctional electrocatalysts in literature.

Catalysts	$E_{1/2}$ (V *vs.* RHE)	$E_{j=10}$ (V *vs.* RHE)	ΔE (V *vs.* RHE)	Power density (mW cm^{-2})	Stability	Ref.
Co/N-CNT	**0.85**	**1.62**	**0.77**	**130**	**1800/1200 h@5 mA cm^{-2}**	**This work**
Co@N-CNT/rGO-0.1	0.82	1.69	0.87	122	125/125 h@5 mA cm^{-2}	[1]
Co-NC-900	0.82	1.69	0.87	115	180/60 h@10 mA cm^{-2}	[2]
Co@NC-3	0.804	1.72	0.916	163.4	450/75 h@10 mA cm^{-2}	[3]
FeCo/N-CNTs@CC	0.816	1.638	0.822	132	65 h@20 mA cm^{-2}	[4]
CoFeNi@CNT	0.82	1.67	0.85	152.3	1500/250 h@5 mA cm^{-2}	[5]
FeCo-Co/NC	0.808	1.583	0.775	120.62	350 h@5 mA cm^{-2}	[6]
NiFe@NCNTs	0.79	1.56	0.77	360.12	200 h@10 mA cm^{-2}	[7]
CN@NC-2-800	0.83	1.63	0.80	172	300/300 h@10 mA cm^{-2}	[8]
Fe-NC/rOCNT	0.865	1.672	0.807	182	1000/1000 h@10 mA cm^{-2}	[9]
m-C@Co/CoO-bC	0.80	1.68	0.88	255	720/120 h@10 mA cm^{-2}	[10]
Co_2P/doped-CNTs	0.843	1.657	0.814	193.3	110 h@10 mA cm^{-2}	[11]
CoFeNi-CNTs	0.85	1.67	0.82	138.7	3000/500 h@5 mA cm^{-2}	[12]
glu-NiFe	0.85	1.67	0.82	127	1440/240 h@5 mA cm^{-2}	[13]
FeOOH-CNT-FeCo/NC	0.79	1.65	0.86	284	686/686 h@10 mA cm^{-2}	[14]
Co-NC+CNT	0.837	1.677	0.84	225	600/200 h@5 mA cm^{-2}	[15]
Co_2P/NP-CNTs	0.81	1.65	0.84	167.03	70 h@2 mA cm^{-2}	[16]
Co_2P@NCNT-4	0.83	1.70	0.87	217	1380/230 h@10 mA cm^{-2}	[17]
Mn_3O_4/NCNTs/Co	0.83	1.62	0.79	128	160/160 h@5 mA cm^{-2}	[18]
NiFe/bNCNT	0.80	1.58	0.78	224	330/330 h@10 mA cm^{-2}	[19]

4. References

[1] Peng X, Wei L, Liu Y, et al. Cobalt nanoparticles embedded in N-doped carbon nanotubes on reduced graphene oxide as efficient oxygen catalysts for Zn-air batteries. *Energy & Fuels*, **2020**, *34(7)*: 8931-8938.

[2] Tang R, Li Y, Liu J, et al. Cobalt nanoparticles embedded nitrogen-doped carbon nanotubes as bifunctional catalysts for flexible solid-state Zn-Air battery. *Journal of The Electrochemical Society*, **2020**, *167(6)*: 060521.

[3] Liu Y, Ji D, Li M, et al. Facile synthesis of cobalt nanoparticles encapsulated in nitrogen-doped carbon nanotubes for use as a highly efficient bifunctional catalyst in rechargeable Zn-Air batteries. *Journal of Alloys and Compounds*, **2020**, *842*: 155791.

[4] Li Z, Yang H, Sun H, et al. Highly nitrogen-doped carbon nanotube nanoarrays as self-supported bifunctional electrocatalysts for rechargeable and flexible zinc-air batteries. *ACS Sustainable Chemistry & Engineering*, **2021**, *9(12)*: 4498-4508.

[5] Chen D, Li G, Chen X, et al. Developing nitrogen and Co/Fe/Ni multi-doped carbon nanotubes as high-performance bifunctional catalyst for rechargeable zinc-air battery. *Journal of Colloid and Interface Science*, **2021**, *593*: 204-213.

[6] Liu X, Peng S, Li X, et al. Encapsulation of FeCo-Co nanoparticles in N-doped carbon nanotubes as bifunctional catalysts for Zn-air battery. *Journal of The Electrochemical Society*, **2021**, *168(9)*: 090514.

[7] Jiang M, Tan Z, Cao M. A robust bifunctional electrocatalyst for rechargeable zinc-air batteries: NiFe nanoparticles encapsulated in nitrogen-doped carbon nanotubes. *International Journal of Hydrogen Energy*, **2021**, *46(29)*: 15507-15516.

[8] Zhu Z, Xu Q, Ni Z, et al. CoNi nanoalloys @ N-doped graphene encapsulated in N-doped carbon nanotubes for rechargeable Zn-air batteries. *ACS Sustainable Chemistry & Engineering*, **2021**, *9(40)*: 13491-13500.

[9] Sheng J, Zhu S, Jia G, et al. Carbon nanotube supported bifunctional electrocatalysts containing iron-nitrogen-carbon active sites for zinc-air batteries. *Nano Research*, **2021**, *14*: 4541-4547.

[10] Lee J Y, Park G D, Kim J H, et al. Synthesis of three-dimensional Co/CoO/N-doped carbon nanotube composite for zinc air battery. *International Journal of Energy Research*, **2021**, *45(11)*: 16091-16101.

[11] Song L, Fan H, Fan X, et al. A simultaneous phosphorization and carbonization strategy to synthesize a defective Co_2P/doped-CNTs composite for bifunctional oxygen electrocatalysis. *Chemical Engineering Journal*, **2022**, *435*: 134612.

[12] Chen D, Li G, Chen X, et al. CoFeNi/N-codoped carbon nanotubes with small diameters derived from spherical Prussian blue analog as bifunctional oxygen electrocatalysts for rechargeable Zn-air batteries. *Journal of Alloys and Compounds*, **2022**, *910*: 164964.

[13] Chen X, Chen D, Li G, et al. FeNi incorporated N doped carbon nanotubes from glucosamine hydrochloride as highly efficient bifunctional catalyst for long term rechargeable zinc-air batteries. *Electrochimica Acta*, **2022**, *428*: 140938.

[14] Yang P Q, Ko T E, Tseng C M, et al. FeOOH-carbon nanotube-FeCo/nitrogen-doped porous carbon as an excellent bifunctional catalyst for achieving high power performance in rechargeable zinc-air batteries. *Journal of Industrial and Engineering Chemistry*, **2023**, *121*: 338-347.

[15] Yang H, Yi X, Fan F, et al. Co single atoms building bifunctional catalysts for zinc-air batteries. *Materials Letters*, **2023**: 134590.

[16] Sun T, Li T, Han D, et al. N, P-doped carbon nanotubes encapsulated with Co_2P nanoparticles as efficient bifunctional oxygen electrocatalysts for rechargeable Zn-air battery. *Journal of Electroanalytical Chemistry*, **2023**, *928*: 117016.

[17] Peng X, Xian X, Han L, et al. Co_2P nanoparticles encapsulated in N-doped carbon nanotubes as a bifunctional oxygen catalyst for a high-performance rechargeable Zn-air battery. *ACS Applied Nano Materials*, **2023**, *6(3)*: 2027-2034.

[18] Lu L N, Chen C, Xiao K, et al. Boosting oxygen electrocatalytic reactions with Mn_3O_4/self-growth N-doped carbon nanotubes induced by transition metal cobalt. *Catalysis Science & Technology*, **2020**, *10(21)*: 7256-7261.

[19] Hong J H, Park G D, Kang Y C. Aerosol-assisted synthesis of bimetallic nanoparticle-loaded bamboo-like N-doped carbon nanotubes as an efficient

bifunctional oxygen catalyst for Zn-air batteries. *International Journal of Energy Research*, **2022**, *46(4)*: 5215-5225.